
Audiomagnetotelluric survey at the Bañitos-Gollete geothermal area, main Andes Cordillera of San Juan, Argentina

H. BARCELONA¹ G. PERI² D. WINOCUR¹ A. FAVETTO³

¹CONICET-IDEAN, Instituto de Estudios Andinos, Universidad de Buenos Aires
Pabellón II, Núñez, Buenos Aires, C1428EHA. Barcelona: h.lidenbrock@gmail.com

²CONICET-IGEBA, Instituto de Geociencias Básicas, Aplicadas y Ambientales de Buenos Aires, Universidad de Buenos Aires
Pabellón II, Nuñez, Buenos Aires, C1428EHA

³CONICET-INGEIS, Instituto de Geocronología y Geología Isotópica-CONICET, Buenos Aires
Pabellón INGEIS, Ciudad Universitaria, C1428EHA

ABSTRACT

The present research explores the Bañitos-Gollete geothermal field located in the Frontal Andes Cordillera over the Pampean flat-slab. We carried out an audiomagnetotelluric survey in order to define the underground geoelectrical structure and to understand the link between the geothermal fluid flow path and the main geological structures. 2-D audiomagnetotelluric models suggest that the deep-rooted N-S fault system controls the geothermal flow path. We propose a conductive heat-driven system, taking into consideration the geologic setting and the supposed low geothermal gradient of this tectonic environment. The mature Na-Cl waters from Gollete and an estimated reservoir temperature of ~140°C are consistent with this conceptual model. Further investigations are required to assess the geothermal potential of the study area, and the present work likely represents only the first but necessary step in the exploration process.

KEYWORDS | Audiomagnetotellurics. Geothermal resource. Hydrothermal system. Valle del Cura basin. Andes.

INTRODUCTION

The study zone is located in the Valle del Cura, in the Argentine Frontal Cordillera over the Pampean flat-slab segment (Fig. 1A). This valley is famous for their economic mineralization resources formed during intense Oligocene to Miocene hydrothermal-magmatic episodes (Bissig *et al.*, 2001, 2002, 2003; Kay *et al.*, 1999; Kay and Coira, 2009). The last main volcanic activity (lower-middle Miocene) originated the basaltic deposits of the Cerro de las Tórtolas Formation (Maksaev *et al.*, 1984).

Additionally, a small volcanic event (1.5–2.0Ma) occurred a few hundred meters north of the main thermal area of Valle del Cura (Despoblados area). The lack of recent volcanic activity contrasts with the various active hydrothermal manifestations present in Valle del Cura.

A total of seven active thermal zones along 60km in a N-S trend were identified in Valle del Cura (Fig. 1B). These zones are constrained by the Zancarrón and La Brea ridges. Pesce and Miranda (2003) compiled geochemical information on these zones, providing temperature

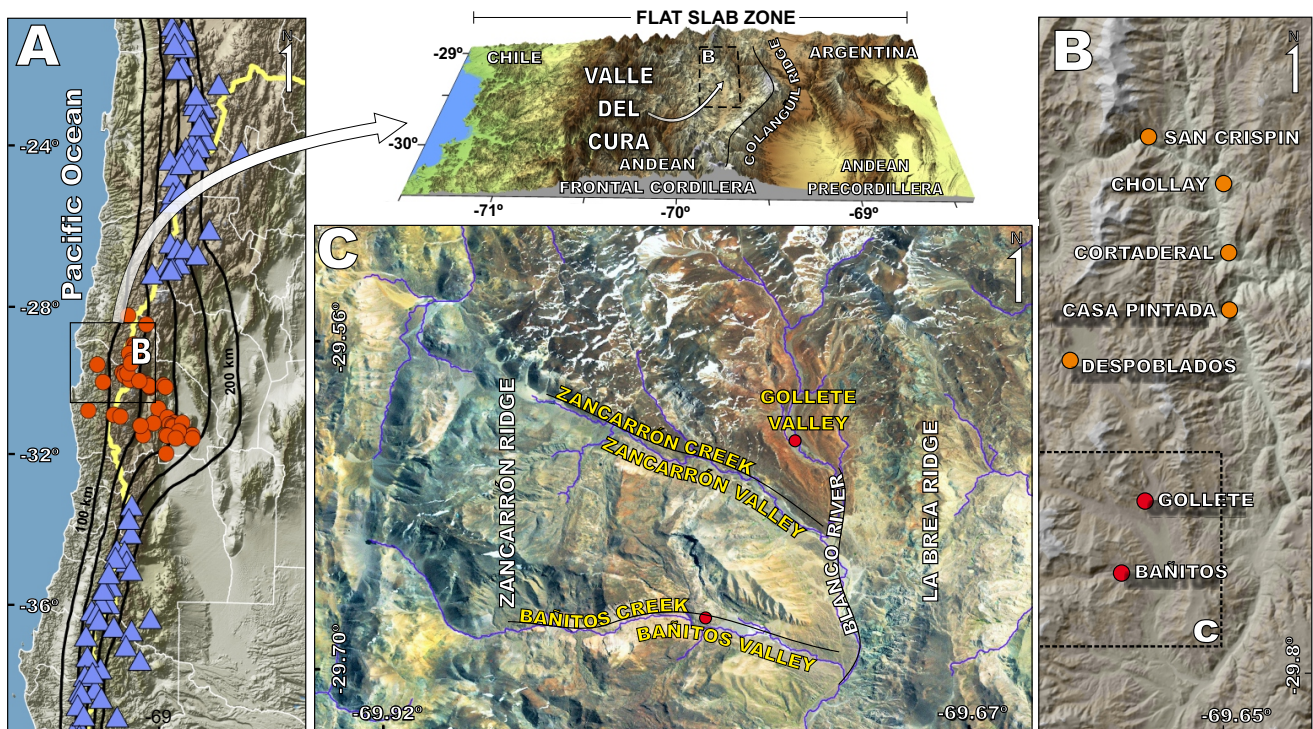


FIGURE 1. A) Location of the Valle del Cura Basin (black square) over the Pampean flat-slab segment in the Andean Cordillera, and location of Holocene active volcanoes (blue triangles; from Smithsonian Institution, Global Volcanism Program) and thermal springs (red circles) in the Pampean flat-slab (Pesce and Miranda, 2003; Risacher and Hauser, 2008). Slab depth contours from Syracuse and Abers (2006). B) Distribution of thermal areas in the Valle del Cura Basin. C) Detailed topographic features of the study zone.

estimations ranging from 180–200°C, but they did not perform an extensive analysis. A geothermal model for the Despoblados area using magnetotelluric data has been proposed by Barcelona *et al.* (2014). However, no preliminary models for the northern and southern geothermal zones exist.

The magnetotelluric method is commonly applied in exploration studies of geothermal systems because it is sensitive to the presence of fluids (Spichak and Manzella, 2009). The main objective is to define the electrical resistivity present at depth and to infer the geologic structure and elements of the geothermal system, such as the source and pattern of fluid flow and location of reservoirs (e.g. Bertrand *et al.*, 2013; Bibby *et al.*, 2009; Blake *et al.*, 2016; Muñoz, 2013; Newman *et al.*, 2008). The combination of geophysics and geological data is a handy tool for the characterization and exploitation of geothermal/hydrothermal systems.

The focus of this study is on the southern geothermal zones located in the Bañitos and Gollete valleys, between the Zancarrón and La Brea ridges (Fig. 1C). We performed an audiomagnetotelluric survey to define the underground geoelectrical structure and to analyze the relation between the thermal fluid path and the geological setting. This

study aims to supply a preliminary conceptual model for the Bañitos and Gollete geothermal zones.

GEOLOGICAL SETTING

The Valle del Cura basin constitutes a 100km long and 40km wide morphostructural segment that is dominated by a consequent valley with an N-S trend. It is located to the west of the Andean Precordillera and extends from the Colangüil Cordillera in Argentina to the Atacama-Coquimbo region in Chile (see Fig. 1). Because of the Miocene flattening of the subducted slab, the Valle de Cura exhibits a thick skin deformation style dominated by the tectonic inversion of Oligocene extensional faults (Alonso *et al.*, 2011; Bissig *et al.*, 2001; Bissig *et al.*, 2003; Godoy *et al.*, 1999; Jordan and Allmendinger, 1986; Mpodozis and Ramos, 1989; Ramos *et al.*, 1989; Ramos, 2010). The structural trend is N-S and is partially overlapped by pre-Andean N120° lineaments that may control the propagation of the thrusts. The Zancarrón and Bañitos valleys are likely an expression of these basement lineaments.

Several authors have studied the geology of the Zancarrón, Gollete and Bañitos valleys (Malizia *et al.*, 1997; Limarino *et al.*, 1999; Litvak and Poma, 2005; Litvak,

2009; Winocur, 2010). Figure 2A shows the distribution of the geological units in the studied area. Permo-Triassic rhyolite deposits constitute the basement, overlaid by a thick Oligocene sequence of dacitic, rhyolitic ignimbrites, lava flows and andesitic lavas of the Tilto and Escabroso formations (Maksaev *et al.*, 1984; Winocur *et al.*, 2014). The concomitant clastic and volcanoclastic facies are grouped in the Valle del Cura Formation (Limarino *et al.*, 1999; Litvak and Poma, 2005; Malizia *et al.*, 1997). Miocene basalts of the Cerro de las Tórtoras Formation (Maksaev *et al.*, 1984) and sandstones of the Bañitos Formation (Limarino *et al.*, 1999) coronate the stratigraphic column.

Figure 2B shows the geological cross-section of the Zancarrón Valley that synthesizes the structural setting of the Bañitos and Gollete thermal zones. The older high-angle thrust fault is located to the east of the Gollete Valley and corresponds to the uplift of La Brea Ridge (Limarino *et al.*, 1999). Two main deformation pulses formed the Zancarrón Ridge. The first pulse developed the western high-angle thrust fault located in the Taguas Valley at 12Ma (Nullo y Marin, 1990) and the second pulse, the last deformation pulse in the region, occurred during the Pliocene-Pleistocene (Limarino *et al.*, 1999). These two deformation stages indicate that the same structural framework controlled the development of

the Bañitos, Zancarrón and Gollete valleys, suggesting that they may be part of the same geothermal system. However, some local structures in the western slope of La Brea Ridge may differentially interfere with the Gollete hot springs. It is interesting to note that both the Oligocene and Miocene volcanic deposits are above the Cretaceous volcanic rocks of the basement domain in the upper 6km crust, according to the structural sections of the region and magnetotelluric data (Barcelona *et al.*, 2014; Winocur, 2010; Winocur and Ramos, 2011; Winocur *et al.*, 2014). Also, the high-angle thrust fault that segments the Zancarrón ridge exposes the sequence of lithostratigraphic units which form the first 500-700m depth below the Gollete valley (Fig. 2C).

GEOHERMAL MANIFESTATIONS

The main thermal springs are located in the western side of the Gollete Valley, above the sandstones of the Bañitos Formation and the tuffs of the Valle del Cura Formation (see Fig. 2A). The Gollete thermal manifestation is associated with an incrustation cone of 11m in altitude (Fig. 3A). The horizontal section is an ellipsoid 147m in circumference with a 33m long minimum axis and a 56m long maximum axis with a N297° trend. The elongate shape suggests a structural

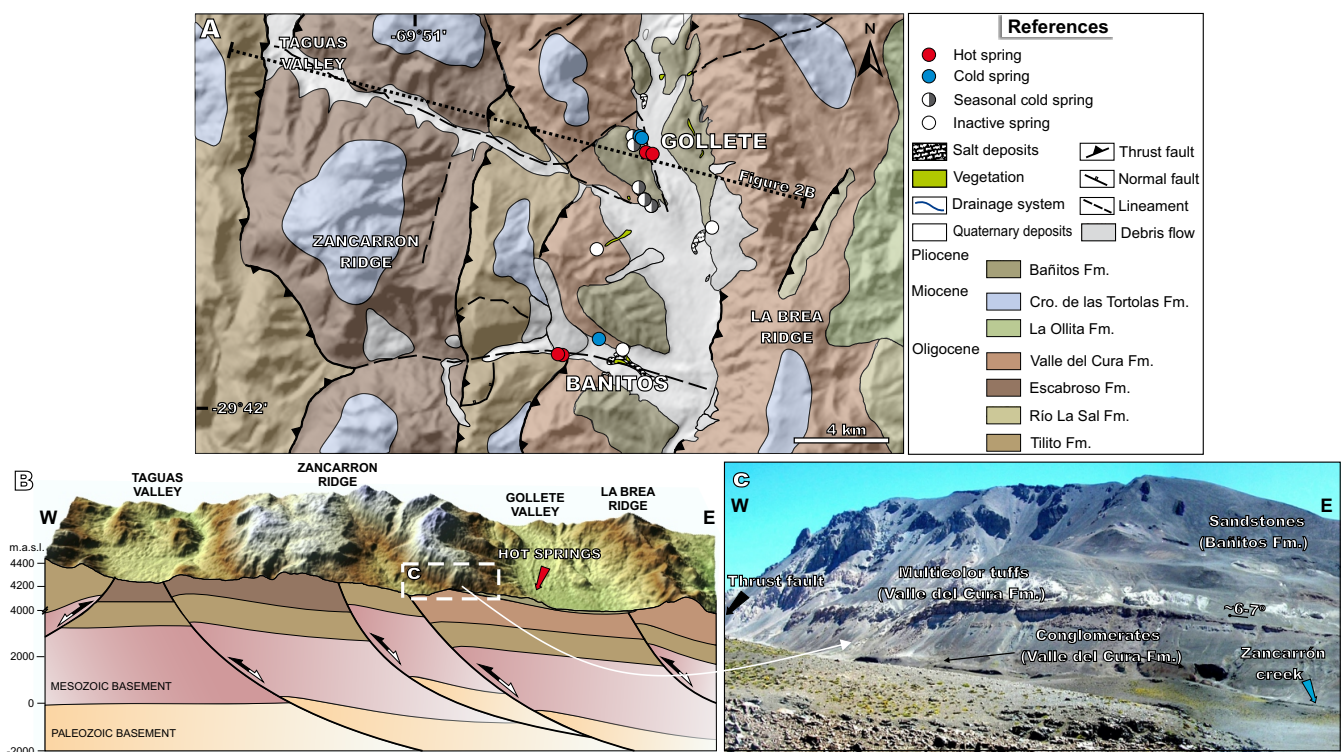


FIGURE 2. A) Geologic map of Bañitos, Zancarrón and Gollete valleys based on Litvak and Poma (2005), Malizia *et al.* (1997), Winocur *et al.* (2014) and field data, satellite images and digital elevation model interpretations. B) Interpreted structural section of Zancarrón Valley, from its head at Taguas Valley (Argentina-Chile frontier) to La Brea Ridge. The red arrow shows the position of the Gollete main hot spring. The black-white arrows indicate the inversion of previous normal faults. White dashed rectangle indicate the location of Figure 3C. C) North view of the Valle del Cura and Bañitos formations that the high-angle thrust fault exposed when it segmented the Zancarrón Ridge.

control, and the Gollete site might be a little travertine fissure ridge. At the top of the cone, there is a $\sim 60^{\circ}\text{C}$ thermal spring with vigorous gas flux. Other seasonal cold springs, commonly associated with mud pools, are also distributed in the southern hill slope of the Zancarrón Valley, close to the outlet of the homonymous creek (Fig. 3B). The cold springs develop above the tuffs and erode both the sandstones of the Bañitos Formation and the Quaternary deposits. Two pools and several hot springs with a temperature above 40°C compose the southern Bañitos thermal area. The hot springs are placed at the foot of debris flows along both sides of Bañitos Creek (Fig. 3C). The host rock is represented in the north by mass transport deposits and in the south by Oligocene volcanic deposits and travertine terraces.

We used available data from the thermal water catalog of Pesce and Miranda (2003) to perform a brief characterization of the fluid discharge in these thermal zones. Na-Cl is the dominant hydrochemical water type in the geothermal waters (Fig. 4A, B). In the $\text{HCO}_3\text{-Cl-SO}_4$ ternary diagram, thermal waters from Gollete are clustered at the mature waters field, which, suggests low interaction with cold meteoric waters during upwelling. Considering the chloride content as a chemical conservative, the spread of Bañitos waters indicates a mixing with shallow cold groundwater during their ascent to the surface.

Empirical and theoretical chemical thermometry was used to estimate the reservoir temperature. Figure 4C shows that all the waters from Gollete locate at the partially equilibrated or mixed waters field and including the Bañitos waters locate at the Na-K 220°C equilibrium curve. This value must be interpreted with caution because i) the Bañitos waters are immature waters and show a mixing trend and ii) the temperature appears to be higher than predictable from geological observations (*e.g.* lack of high-temperature hydrothermal alteration at the surface). Silica geothermometers perform more accurate temperature estimations in these conditions. Thus, an alternative reservoir temperature estimation was calculated by the K-Mg- SiO_2 geothermometer proposed by Giggenbach *et al.* (1994). Figure 4D shows that the waters from Gollete adjust to a conductive cooling from a 130°C source.

AUDIOMAGNETOTELLURIC DATA ACQUISITION AND SIGNAL PROCESSING

A total of fifty-eight audiomagnetotelluric sites were sampled using a Geometrics Stratagem data logger with a standard procedure. We used BF6 and BF4 sensors from Geometrics to measure the horizontal magnetic field,

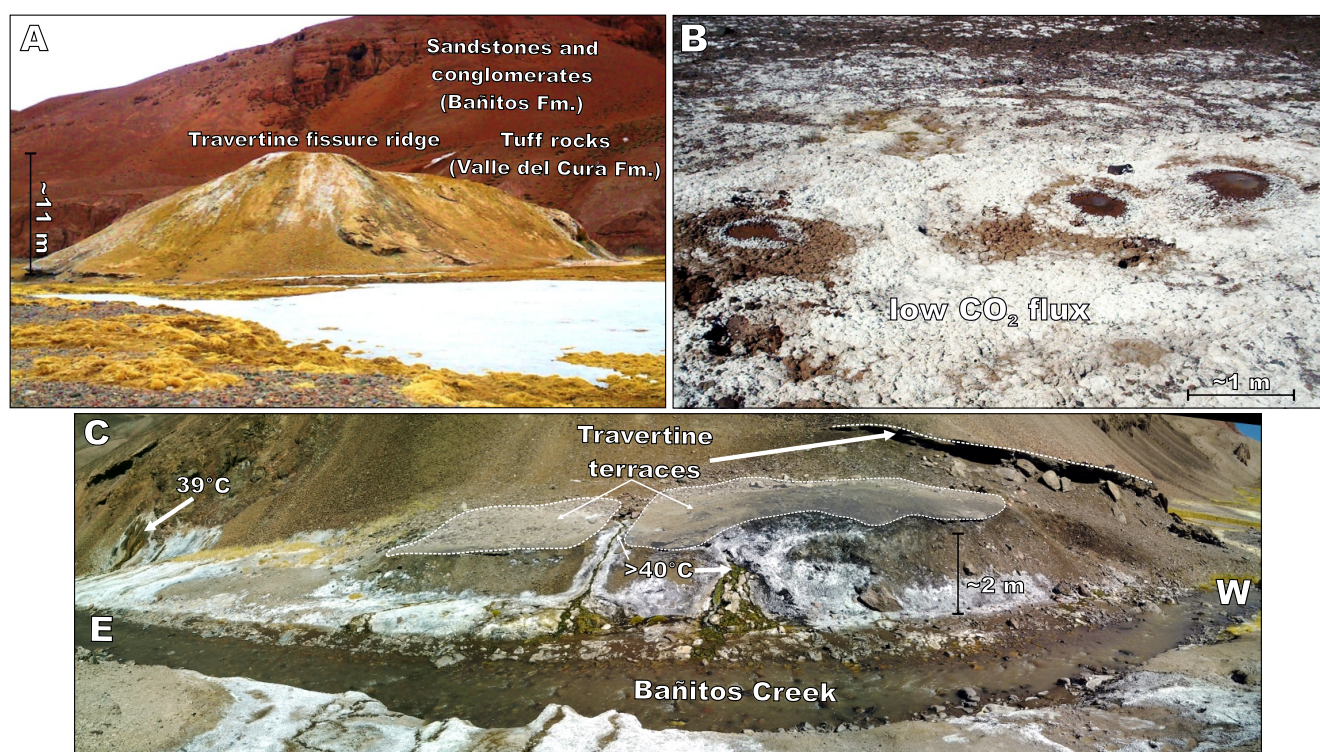


FIGURE 3. Main geothermal manifestations in the Bañitos-Gollete geothermal areas. A) The fissure ridge called Gollete. B) Mud pools related to cold springs in the eastern part of the Zancarrón Valley. Note the intense carbonaceous precipitation that characterizes the entire thermal zone. C) Thermal springs and travertine terraces in the Bañitos geothermal zone.

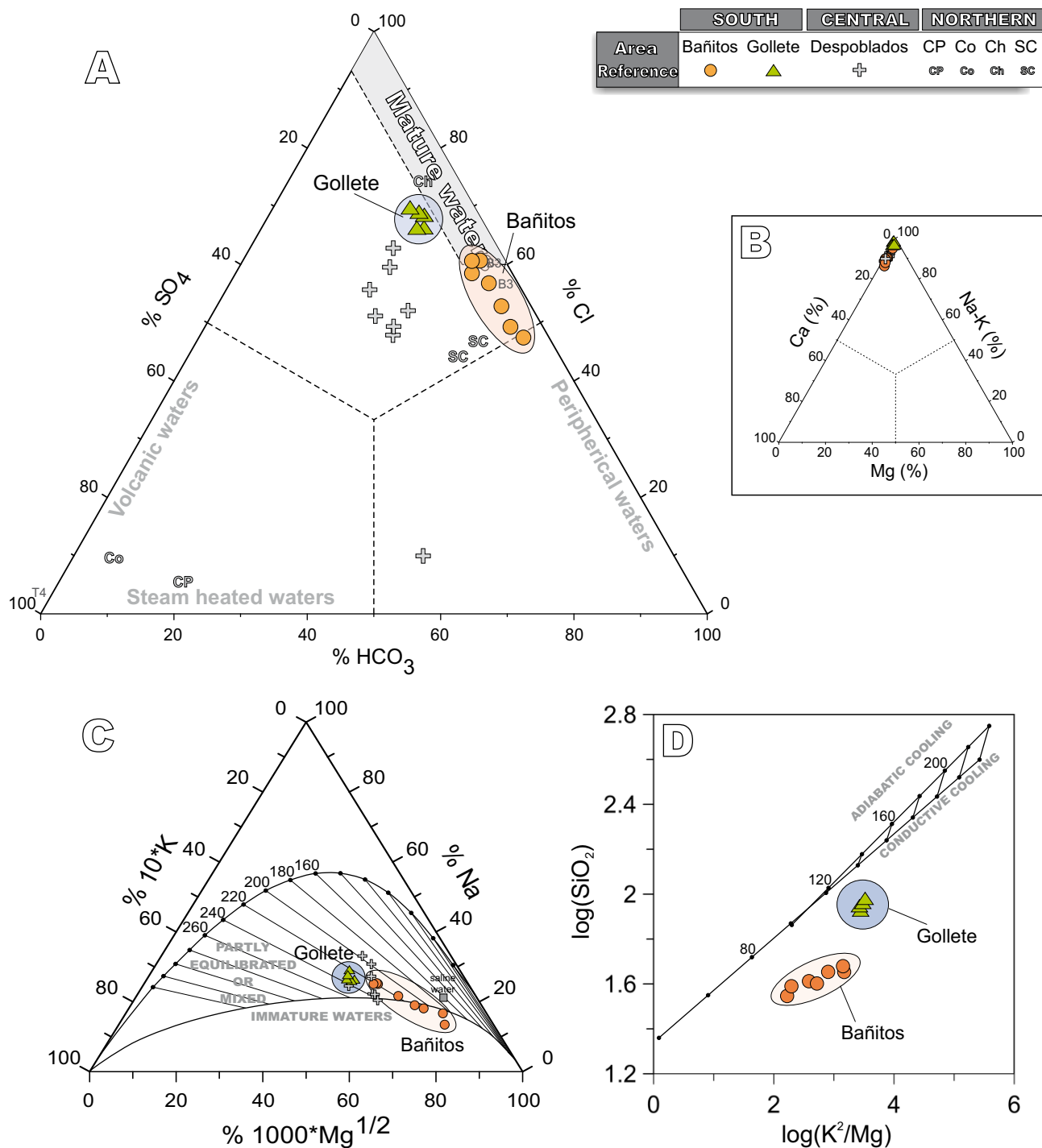


FIGURE 4. Hydrochemical characterization and geothermometry for the Bañitos-Gollete geothermal waters (chemical data from [Pesce and Miranda, 2003](#)). A) Ternary diagram for the systems SO₄-Cl-HCO₃ ([Ellis et al., 1964](#)). Central and northern hot springs are included for reference. B) Cation ternary diagram Ca-Na + K-Mg. C) Na-K-√Mg ternary diagram ([Giggenbach, 1988](#)). D) log(K²/Mg) vs. log(SiO₂) from [Giggenbach et al. \(1994\)](#).

and two 60m dipoles with conventional non-polarizable electrodes oriented N-S and E-W ([Fig. 5](#)). The registered frequency band for the study ranged from 1Hz to 1000Hz; however, depending on the curve features obtained, the range increased to 3000–0.3Hz.

We focused the AMT sampling roughly on the E-W Bañitos and Zancarrón valleys and the broader N-S Gollete Valley, according to the structure and geological characteristics of the area. The sites are approximately 500m apart, and the final distribution of the three study zones is shown in [Figure 6](#).

Geometrics Image software was used to control the recording and in-situ data pre-processing and processing. Filtering of signal, gain setting for each channel (magnetic and electric fields) and calculation of the complex tensor impedance (Z) were the standard procedures in the field. More than fifty-time series segments from each frequency band were stacked automatically for robust analysis to enhance the signal-noise ratio. The value of the coherence threshold selected for the electric and magnetic fields was 0.7. After the fieldwork, data were again analyzed. A manual selection of the time series segment was chosen, and the threshold selected for the electric and magnetic fields was increased to 0.9 to obtain high-quality data.

DIMENSIONALITY AND STRIKE ANALYSIS

Asymmetry parameters estimated the distortion and dimensionality of the impedance tensor. The skew_{swift} is the conventional asymmetry parameter based on the Z magnitude as defined by Swift (1967). Another standard asymmetry parameter is the phase sensitive skew (skew_{bahr}) that is calculated by taking into account the phases because it is less sensitive to surface distortion (Bahr, 1988). The skew_{swift} and the skew_{bahr} are higher than 0.2 and 0.3, respectively, when a significant contribution of a 3D inductive structure is present (Bahr 1991; Reddy et al., 1977). Both skews were used in this study because they are complementary and are required to be below the

respective threshold values to suppose a two-dimensional medium (Berdichevsky and Dmitriev, 2008).

The frequency distributions of both skews for each study zone are shown in Figure 7. The skews show similar behavior with the frequency of the three zones. The value distribution is homogeneous and below the threshold for the 3D medium. A slight increase of the skew dispersion is shown at frequencies below 10Hz. This trend resulted in a small increase of the skews mean value, supposing a slight distortion. This signal effect was expected as it correlates with the dead band decade (*i.e.* the frequency amplitude where the electromagnetic wave intensity is minimal). However, the skews of the three zones are low and suggest no significant distortion present in the signal. Thus, the general assumption of a 2D medium may be valid over the three study zones.

We performed an impedance tensor decomposition to obtain the regional strike to select the geoelectric strike for each 2D profile (Groom and Bailey, 1989; Smith, 1995). The regional strikes were calculated using the Strike code of McNeice and Jones (2001). A single-site multifrequency analysis was performed without any constraints for the three frequency decades. The strike results from the Zancarrón, Bañitos and Gollete valleys are shown in Figure 8. Results show that for Zancarrón and Bañitos profiles, the strike has a roughly N-S direction, but with some drift at higher frequencies and some specific

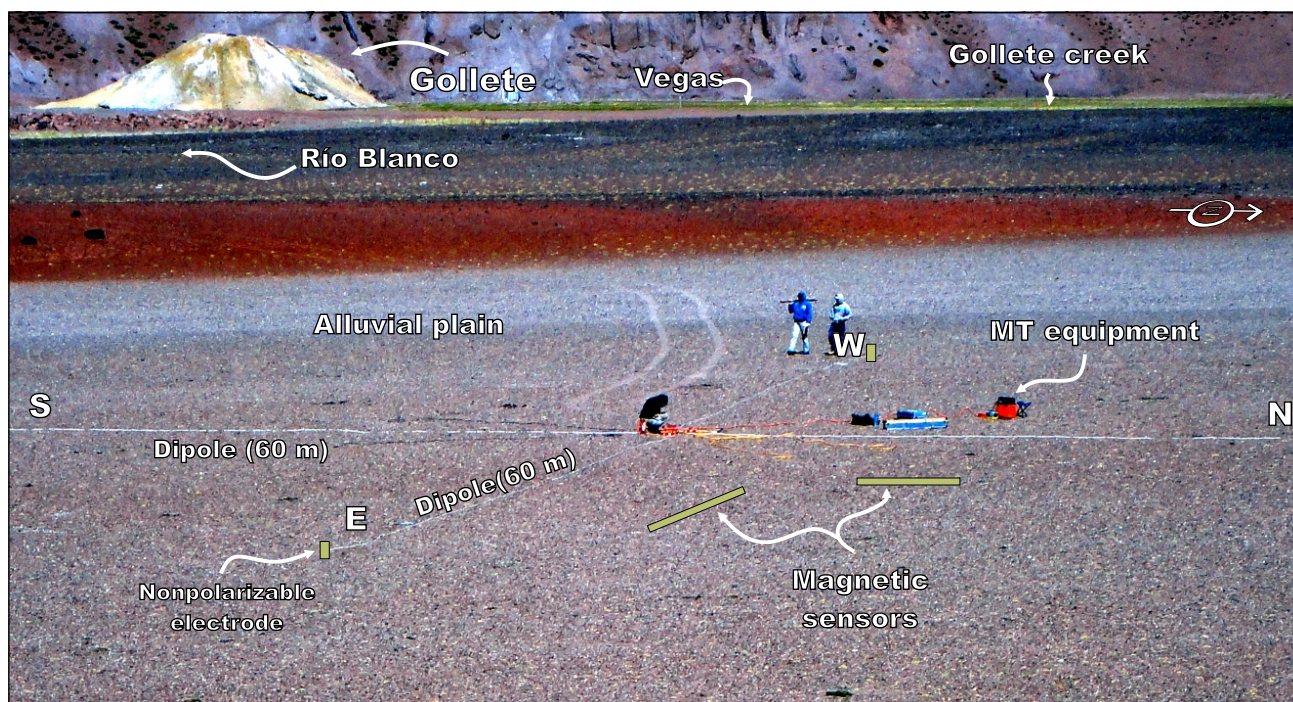


FIGURE 5. Standard audiomagnetotelluric sounding station over the alluvial deposits of Río Blanco. Note the Gollete travertine fissure ridge at the background.

segments of the profiles. Based on the strikes dispersion and audiomagnetotellurics sites distribution, we selected three E-W profiles for 2-D inversions in the Gollete valley.

We performed a multi-site rotation of all frequencies for each profile. The strike was fixed for several angles, and the resultant misfit was analyzed to obtain the mean strike direction for each section. Using this procedure, we ensured that the fits were better for the set of stations. The bar plots of Figure 9 show the misfit (Root Mean Square, RMS) obtained by constrained decomposition as a function of the strike angle. The strike value that corresponds with the lower misfit was selected for each 2D section. Finally, each station was rotated by the selected strike to obtain the final rho and phase curves.

2-D INVERSION SETTINGS

The deterministic approach of the nonlinear conjugate gradient algorithm of Rodi and Mackie (2001), run in the WinGlink software package, was employed to perform the 2-D inversion of AMT data. The grid was built following the recommendations for the maximization of

the algorithm efficiency; the cell dimensions between the stations were increased by a factor of 1.2, by 1.4 away from the stations and 1.2 at depth. No topography was included in the model because the maximum topography difference between stations was lower than 100m. Several starting models were tested, including resistivity distribution, according to the geological models and homogeneous half-space. Lastly, we used the half space starting model of $500\Omega.m$ for the Zancarrón and Bañitos valleys and $100\Omega.m$ for the Gollete Valley because of the lower constraints and the better response of the models.

Both data modes (*i.e.* electric and magnetic transverse) were used during the inversion process, and the standard Laplacian regularization was applied. No discrimination between horizontal and vertical directions of the weighting function was selected. The final error floors for both modes were set to 12% for the apparent resistivity and 5% for phases in all the models. We assigned a higher weight to the phase signal to avoid the potential for no inductive effects related to local and shallow anomalies (Simpson and Bahr, 2005), even though no evidence of this effect was found. Also, the smoothness and the data misfits were analyzed to establish the regularization parameter (τ) for

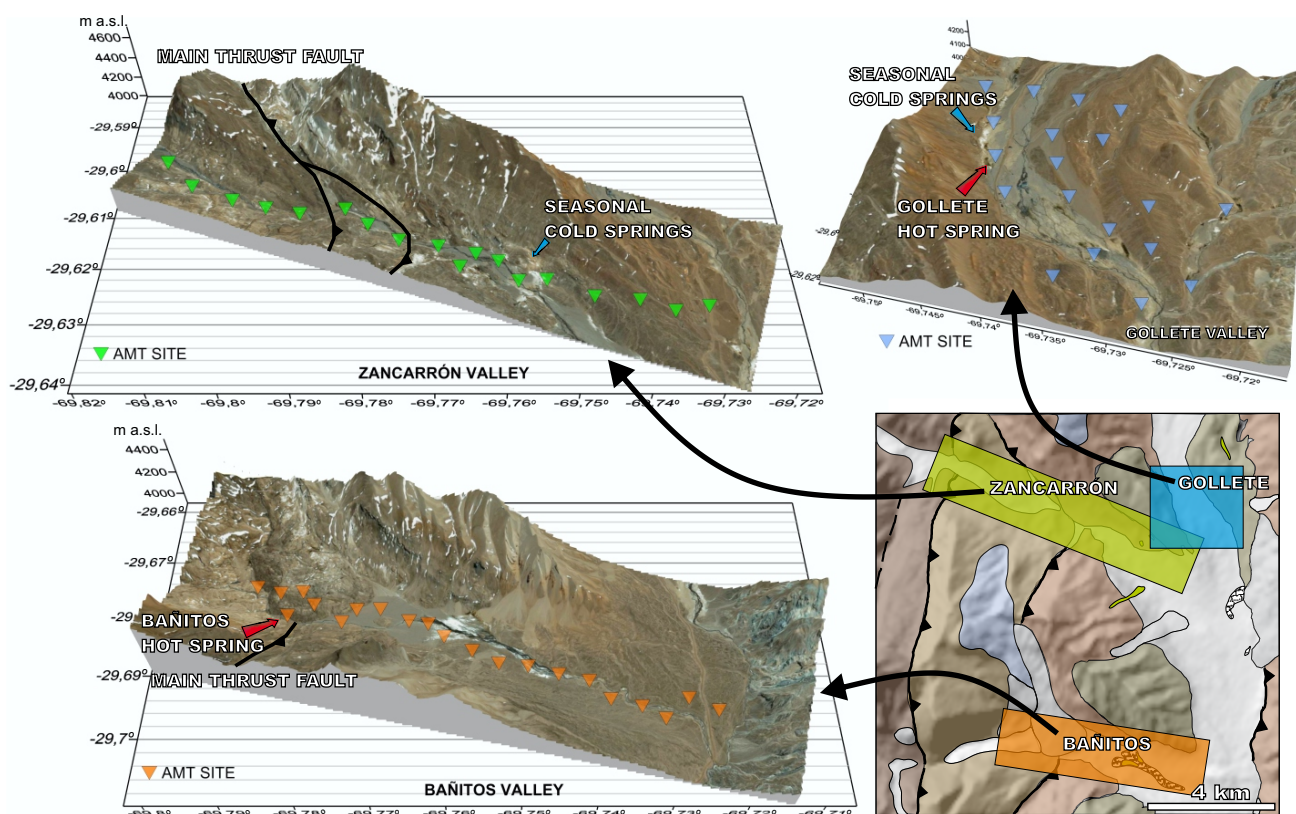


FIGURE 6. Location of the audiomagnetotelluric sites for the three valleys. Colored rectangles plotted over the geologic map (bottom right) indicate the survey areas.

each profile. A regular trade-off curve estimation gave the best fit for τ to be between 8 and 12, depending on the model.

2-D MAGNETOTELLURIC MODELS

The 2-D electric resistivity distribution models of the Bañitos and Zancarrón valleys are shown in Figure 10A and Figure 11A. The mean RMS is of 1.27 and 1.46, respectively, indicating a good fit between the obtained models and the data set (Fig. 10B; 11B). These values are

in agreement with the similarity between the measured and the calculated rho and phase pseudosections (Fig. 10C; 11C). Two main observations could be extracted from the pseudosections. The first one is that the higher resistivity values were measured roughly to the west of the main thrust fault and the lower resistivity values were measured to the east of the main thrust fault (Fig. 10C; 11C). The second one is related to this resistivity distribution that induces skin depth variations and sensitivity changes. The models have higher skin depth and sensitivity in the western sector and decrease to the eastern part of the profiles.

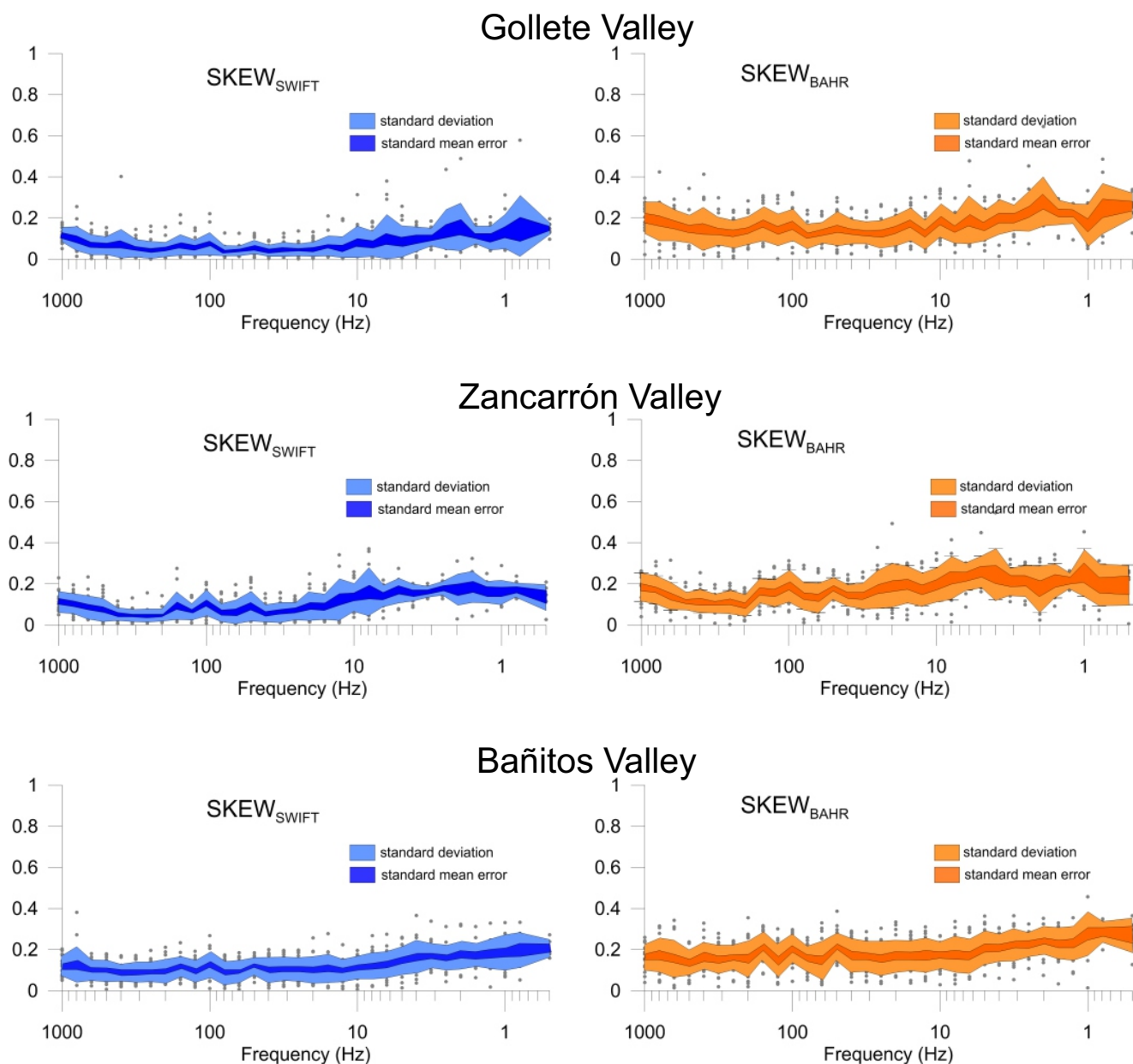


FIGURE 7. Frequency distribution of skew_{swift} and skew_{bahr} for the three study zones.

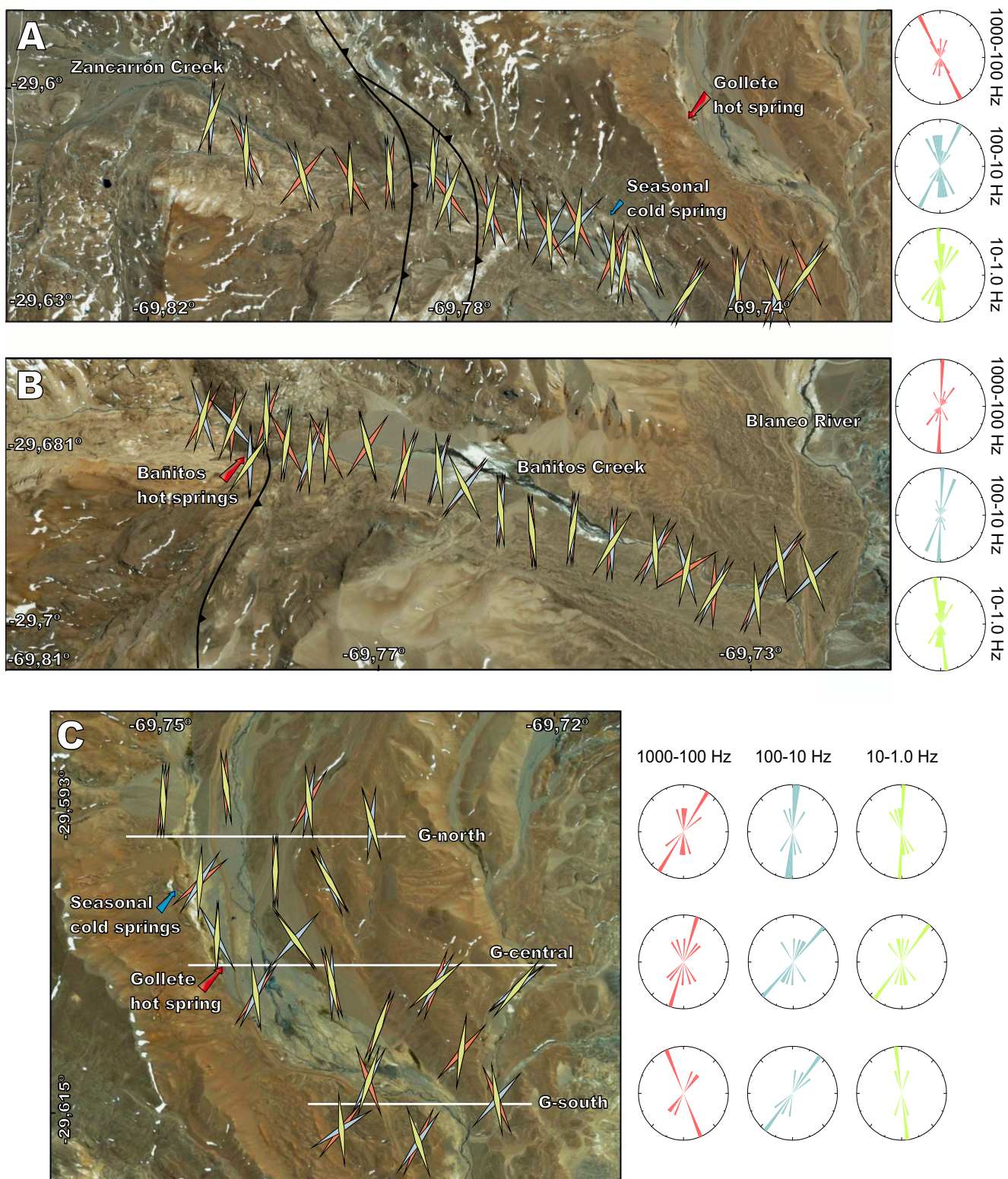


FIGURE 8. Strike directions for the frequency ranges 1000Hz–100Hz, 100Hz–10Hz and 10Hz–1.0Hz for A) Zancarrón, B) Bañitos and C) Gollete valleys. Rose diagrams summarize the strike directions for each frequency range.

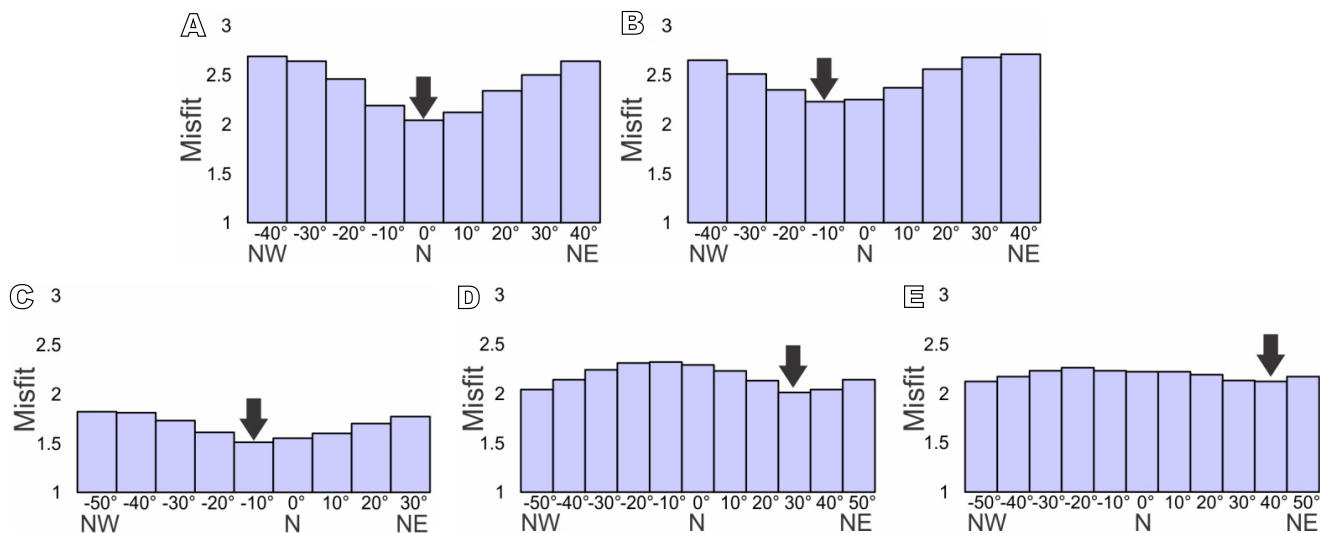


FIGURE 9. Bar plots show misfit (Root Mean Square, RMS) for all sounding stations of A) Zancarrón, B) Bañitos, and C) Gollete North, D) Gollete Central and E) Gollete South. Black arrow indicates the strike selected for the rotation of the measured impedance tensors

Both inversion models define a shallow conductive domain (a) that lies over a basal resistive domain (c). Resistance values in the range of 20–60Ω.m characterize the shallow

conductive domain which forms a wedge to the west with a steady decrease in thickness. Conductive anomalies with resistance values <3Ω.m (b) are found inside this domain.

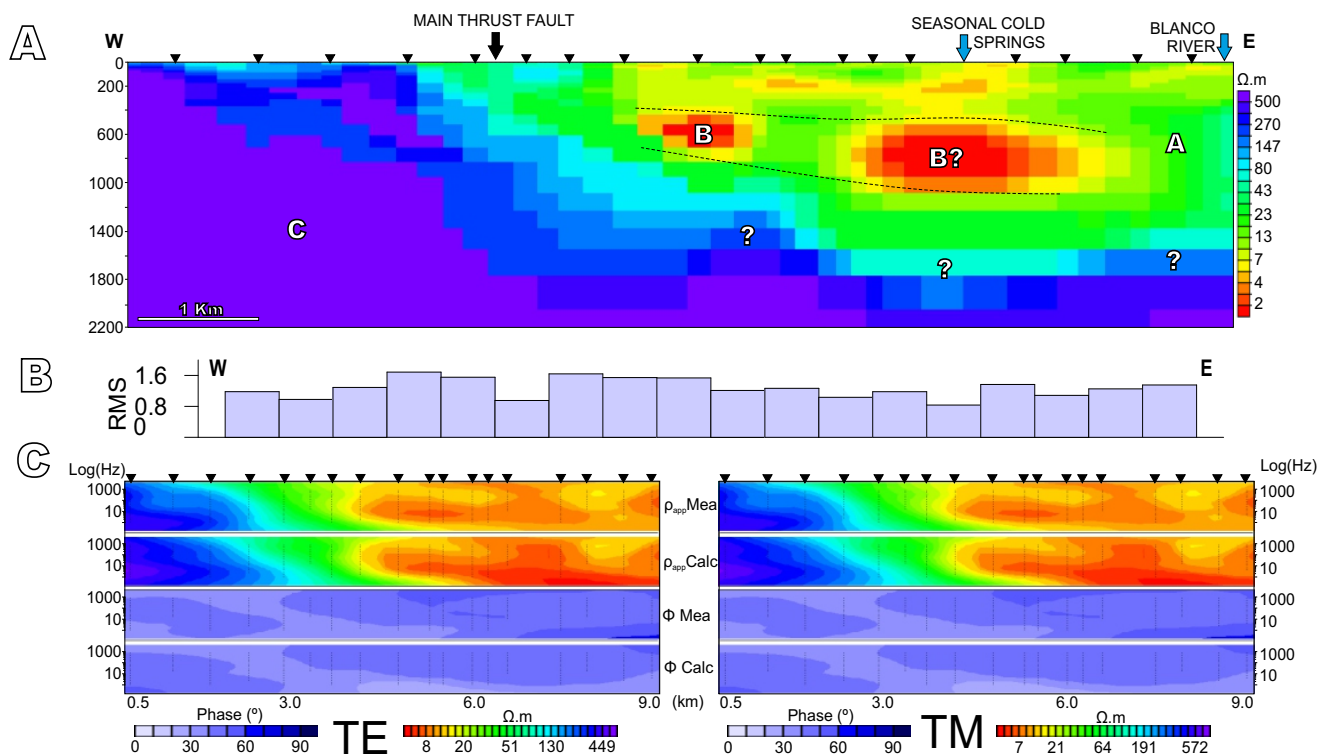


FIGURE 10. A) 2-D electrical resistivity model for the Zancarrón Valley. Black triangles represent the location of audiomagnetotelluric sites. Letters inside the models represent the electrical conductivity domains and anomalies explained in the text. B) Bar plot showing the data fit for each station by the Root Mean Square (RMS) parameter. C) Measured and calculated rho and phase pseudosections for Transverse Electric (TE) and Transverse Magnetic (TM) modes.

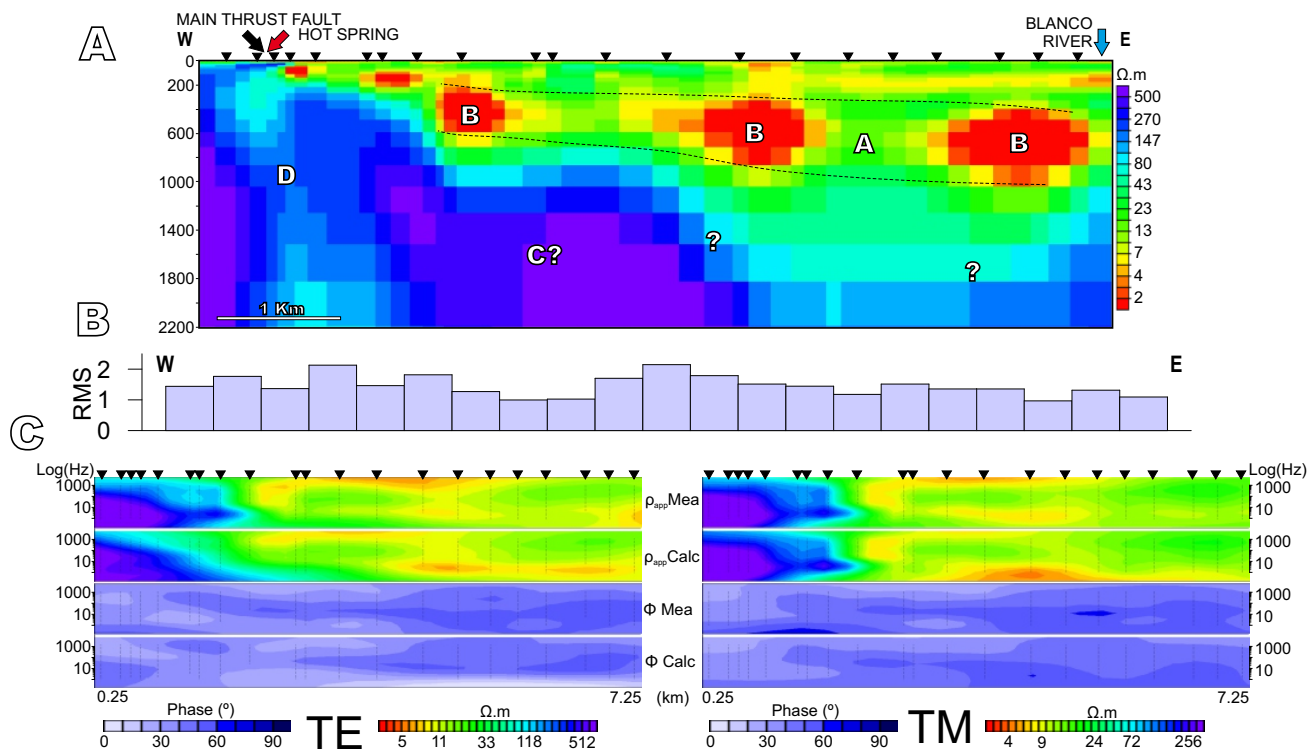


FIGURE 11. A) 2-D electrical resistivity model for the Bañitos valley. Black triangles represent the location of audiomagnetotelluric sites. Letters inside the models represent the electrical conductivity domains and anomalies explained in the text. B) Bars plot that shows the data fit for each station by the Root Mean Square (RMS) parameter. C) Measured and calculated rho and phase pseudosections for Transverse Electric (TE) and Transverse Magnetic (TM) modes

In Zancarrón, the (b) anomalies increase the thickness to the east of the profile, despite some distortion related to a gap in the sounding station distribution (see Fig. 10A); whereas, in Bañitos, the anomalies are composed of several oval-shaped bodies that are aligned and constitute a horizontal geoelectric layer (dashed lines in the profiles). This geoelectric layer is approximately 400m thick and shows a slight inclination to the east, consistent with the 7° inclination of the sequence measured during the fieldwork. This observation is consistent with the lithostratigraphic control over the geoelectric response. It is interesting to note that the western boundary of the shallow geoelectric structure corresponds to the N-S thrust fault trace in both the Bañitos and Zancarrón models, suggesting a structural control over its extension. In fact, in the model of the Bañitos Valley, the thrust fault line correlates with a slight attenuation of the resistivity values (d). This observation suggests that the attenuation defines a subvertical discontinuity through the western resistive geoelectric structure.

The basal resistive domain is characterized by $>200\Omega \cdot m$, it outcrops to the west and continues to the east below the shallow conductive domain. The topography of this domain shows a sequence of steps that determine the plunge of the structure to the east. This topography might be explained by

an antithetic fault system related to the main thrust. However, the validity of this topography at the central and eastern side of the profiles is under debate because of the skin depth and sensitivity variation.

The three 2-D models (Fig. 12) that characterize the electrical resistivity of the Gollete Valley were inverted by the same parameters to facilitate the correlation of the geoelectric structures. The range of the electrical resistivity values in the Gollete Valley is similar to the upper 1000m of the Zancarrón and Bañitos models, which is consistent with the geologic framework (see the structural section in Fig. 2B).

In general, the MT models show that the Gollete valley exhibits a southward progressive simplification of the electrical resistivity distribution, increasing the size and decreasing the number of conductive anomalies ($<3\Omega \cdot m$). Conductive anomalies spread over two levels until a depth of 800m. Pseudosections suggest that these anomalies are the lower sensitivity level of the inversion profiles. The shallower anomalies (e) are located between the first 200m depth and may be related to the Blanco River, whereas the more profound anomalies (f) are located between 400m and 600m depth. Above each conductive level, there are several isolated resistive anomalies (g). Pseudosections

and the relation between the amplitude of the anomaly and the distance between stations suggest that some of these anomalies could be an artifact, but their resistive values and depth are consistent from one model to the other. Finally, the environment around the Gollete hot spring has $\sim 20\Omega.m$ (Fig. 12B), and below 400m depth there is a tabular conductive anomaly (f).

INTERPRETATION

Figure 13A shows the integral model of the Bañitos Valley that was performed crossing the 2D magnetotelluric profiles with the structural cross section of Figure 2B. Alluvial deposits over the tuff and conglomerate levels of the Valle del Cura Formation defines the shallow conductive domain, where the high conductive levels may be a response to the presence of groundwater. On the other hand, the basal resistive domain corresponds to volcanic rocks of low-permeability, affected by the N-S trend fault and an antithetic fault system that puts both domains in tectonic contact. Moreover, the antithetic fault system may be responsible for the compartmentalization of the tilted conductive geoelectrical layer defined by the oval anomalies. The subvertical attenuation of the resistive domain below the Bañitos hot springs confirms not only the

fissure control over the springs and the link with a deep fluid source but also the potential regional role of the faults as a channel for upwelling the fluid flow pattern.

The central 2-D model was interpreted within the geological framework (Fig. 13B). The stratigraphy was based on the descriptions of Malizia et al. (1997) for the west of the profile and through the Zancarrón Valley, where the sequence is exposed. At the bottom, the sequence is composed of 150m thick conglomerates overlaid by 300m of multicolor tuffs and sandstones at the top. As observed in the Bañitos and Zancarrón valleys, the conductive anomalies are not devoid of lithostratigraphic control. The shallower, conductive anomaly level is located at the bottom of the porous sandstones and may be related to the groundwater by surficial water infiltration. Moreover, the bottom conductive anomalies (f) are strictly correlated with the conglomerate level, suggesting that this porous medium has a storage behavior for shallow fluids. Partially welded tuffs with lower permeability are located between both fluid levels, and the resistive anomalies are related to sandstones and clastic tuff without a significant amount of fluids.

The relationship between the conductive anomalies, the fluid, and the hot spring of Gollete is not clear. The dashed

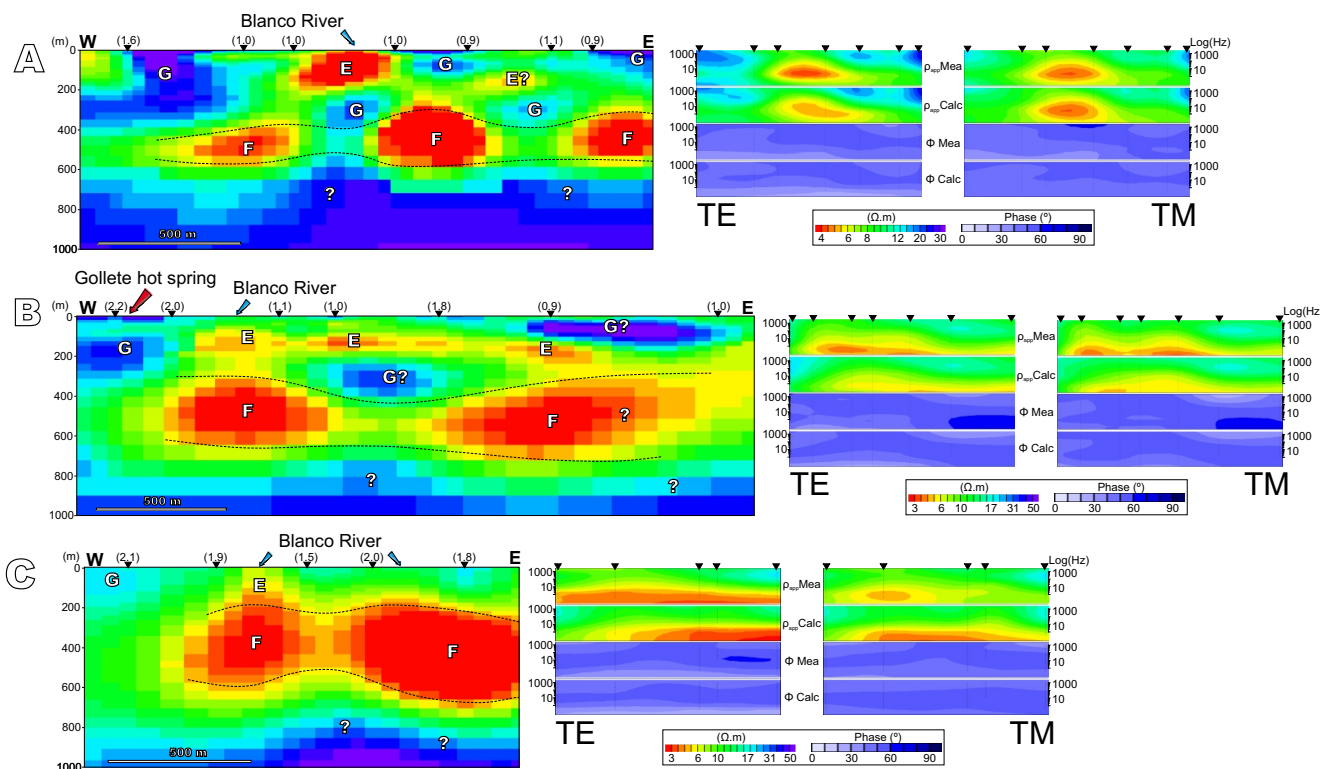


FIGURE 12. 2-D electrical resistivity models for A) northern, B) central and C) southern Gollete Valley. Note that the color scale differs from that in Figures 10 and 11. Black triangles represent the location of MT sites and, above each one, numbers between brackets represent the data fit parameter RMS. Letters inside the models represent the electrical conductivity domains and anomalies explained in the text. To the right of each 2-D model, measured and calculated rho and phase pseudosections for Transverse Electric (TE) and Transverse Magnetic (TM) modes.

red arrows in Figure 13B are the proposed geothermal fluid path (i.e. a vertical path fissure for the upwelling of the thermal fluid through the upper 1000m). Thermal fluid might be partially discharged at the conglomerate layer, producing a mixing zone between thermal fluid and meteoric water, and the remaining fluid then reaches the surface, developing the Gollete hot spring. Additionally, we do not discard a west or northwest location for the main upflow. In this case, the current Gollete position should be subjected to a shallow lateral flowpath.

The lack of lithostratigraphic control at the south of the Gollete Valley might be in response to i) the southeast plunge of the sequence; ii) the higher water infiltration resulting from the Blanco River and Zancarrón Creek intersection, an observation consistent with the mud pools recognized in the zone (Fig. 2A); and iii) a local increase of secondary permeability from fractures.

CONCLUSIONS

The present research aimed to examine for the first time the Gollete-Bañitos geothermal field, located in the Valle del

Cura region (San Juan, Argentina), by performing an extensive shallow audiomagnetotelluric survey. 2D magnetotelluric models for the shallow electrical resistivity distribution of the Bañitos, Zancarrón and Gollete valleys define several geoelectrical structures that directly correlated with the geologic and structural features. The most interesting finding to emerge from this study is that the N-S fault system control on the flow path is confirmed by the proposed models. Hence, a conductive heat-driven system fits with the geologic setting, dominated by a deep circulation over a roughly low geothermal gradient. The mature Na-Cl waters from Gollete and an estimated reservoir temperature of 140°C support this model. It is interesting to note that no conductive geoelectric structure potentially linked to a thermal fluid reservoir was identified at the western side of the study area until a depth of more than 1400m. Unfortunately, the low electrical resistivity response decreased the penetration of the signal to the eastern side of the profile. Also, the shallow conductive geoelectric structures were interpreted as meteoric groundwater, whose emplacement was found to have lithostratigraphic control. Further investigations are required to assess the geothermal potential of the study area and the present work likely represents only the first but necessary step in the exploration process.

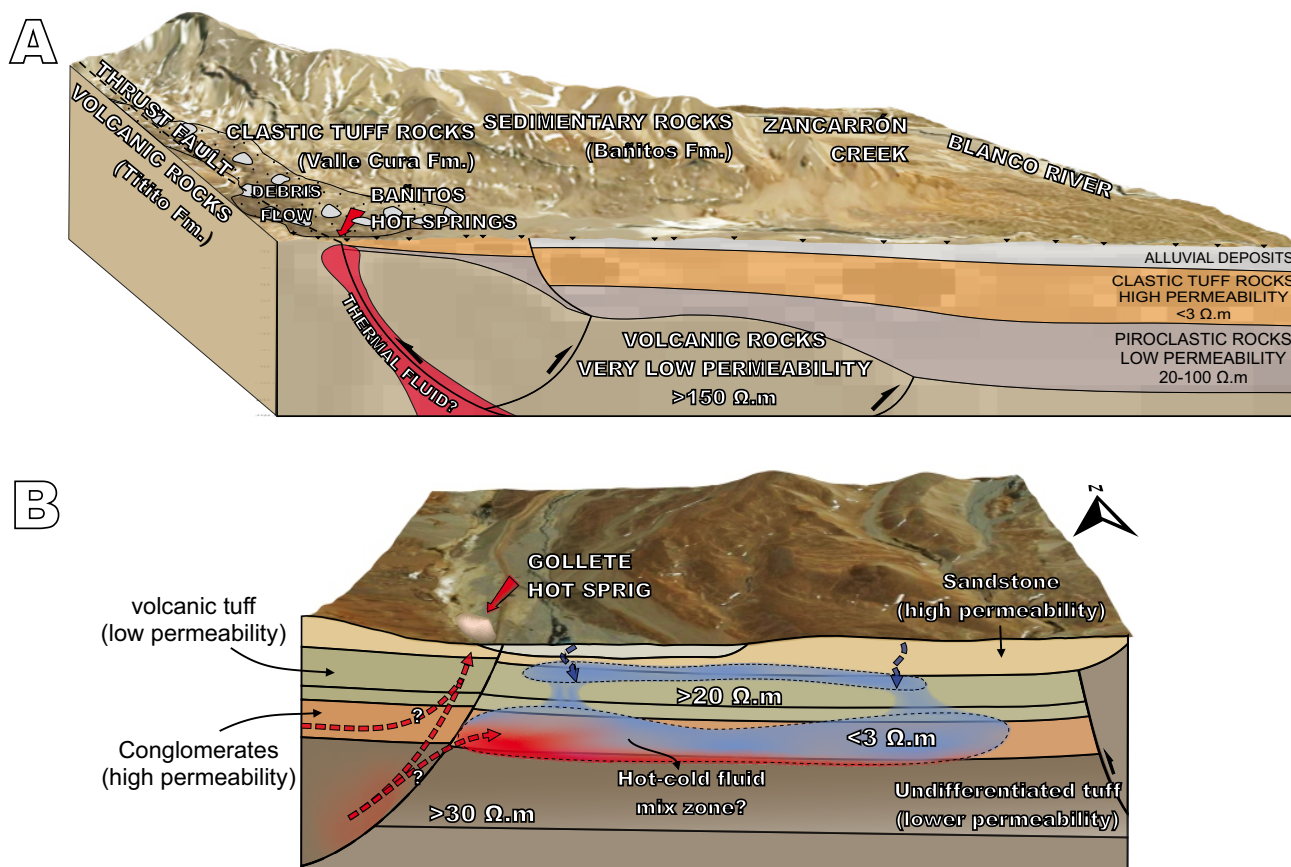


FIGURE 13. The audiomagnetotellurics interpretation model based on the geologic framework for the A) Bañitos and B) Gollete geothermal areas.

ACKNOWLEDGEMENTS

We are grateful to G. Giordanengo, a technician from CONICET, for providing logistical support during the magnetotelluric fieldwork.

REFERENCES

- Alonso, S., Limarino, C., Litvak, V., Poma, S., Suriano, J., Remesal, M., 2011. Palaeogeographic, magmatic and palaeoenvironmental scenarios at 30°SL during the Andean Orogeny: Cross sections from the volcanic-arc to the orogenic front (San Juan province, Argentina). In: Salfity, J.A., Marquillas, R.A. (eds.). *Cenozoic Geology of the Central Andes of Argentine*, SCS Publisher, Salta, 23-45.
- Bahr, K., 1988. Interpretation of the magnetotelluric impedance tensor: regional induction and local telluric distortion. *Journal of Geophysics*, 62, 119-127.
- Bahr, K., 1991. Geological noise in magnetotelluric data: a classification of distortion types. *Physics of the Earth and Planetary Interiors*, 66, 24-38.
- Barcelona, H., Favetto, A., Peri, A., Pomposiello, C., 2014. Sistema geotermal de Despoblados determinado a partir de datos magnetotéluricos, Valle del Cura, San Juan. *Revista de la Asociación Geológica Argentina*, 71(4), 562-574.
- Berdichevsky, M., Dmitriev, V., 2008. *Models and Methods of Magnetotellurics*. Berlin, Springer, 564pp.
- Bertrand, E., Cadwell, T., Hill, G., Bennie, S., Soengkonon, S., 2013. Magnetotelluric imaging of the Ohaaki geothermal system, New Zealand: Implications for locating basement permeability. *Journal of Volcanology and Geothermal Research*, 268, 36-45.
- Bibby, H., Risk, G., Caldwell, T., Heise, W., 2009. Investigations of deep resistivity structures at the Wairakei geothermal field. *Geothermics*, 38, 98-107.
- Bissig, T., Clark, A., Lee, J., Heather, K., 2001. The cenozoic history of volcanism and hydrothermal alteration in the Central Andean flat-slab region: New ⁴⁰Ar-³⁹Ar constrains from the El Indio-Pascua Au (-Ag, Cu) belt, 29°20'-30°30" S. *International Geology Review*, 43, 312-340.
- Bissig, T., Clark, A., Lee, J., Hodgson, C., 2002. Miocene landscape evolution and geo- morphological controls on epithermal processes in the El Indio-Pascua Au-Ag-Cu belt, Chile and Argentina. *Economic Geology*, 97, 971-996.
- Bissig, T., Clark, A.H., Lee, J.K.W., von Quadt, A., 2003. Petrogenetic and metallogenetic responses to Miocene slab flattening: New constrains from the El Indio-Pascua Au-Ag-Cu Belt, Chile/Argentina. *Mineralium Deposita*, 38, 844-862.
- Blake, S., Henry, T., Muller, M.R., Jones, A.G., Moore, J.P., Murray, J., Rath, V., 2016. Understanding hydrothermal circulation patterns at a low-enthalpy thermal spring using audio-magnetotelluric data: A case study from Ireland. *Journal of Applied Geophysics*, 132, 1-16.
- Ellis, A.J., Mahon, W.A.J., 1964. *Chemistry and Geothermal System*. Natural hydrothermal systems and experimental hot-water/rock interactions. *Geochimica et Cosmochimica Acta*, 28(8), 1323-1357..
- Giggenbach, W.F., 1988. Geothermal solute equilibria. Derivation of Na-K-Mg-Ca geothermometers. *Geochimica et Cosmochimica Acta*, 52, 2749-2765.
- Giggenbach, W.F., Sheppard, D.S., Robinson, B.W., Stewart, M.K., Lyon, G.L., 1994. Geochemical structure and position of the Waiotapu geothermal field, New Zealand. *Geothermics*, 23, 599-644.
- Godoy, E., Yañez, G., Vera, E., 1999. Inversion of an Oligocene volcano-tectonic basin and uplift of its superimposed Miocene magmatic arc in the Chilean Central Andes: first seismic and gravity evidences. *Tectonophysics*, 306, 217-236.
- Groom, R.W., Bailey, R.C., 1989. Decomposition of magnetotelluric impedance tensors in presence of local three-dimensional galvanic distortion. *Journal of Geophysical Research*, 94, 1913-1925.
- Jordan, T., Allmendinger, R., 1986. The Sierras Pampeanas of Argentina: a modern analogue of Rocky Mountain foreland deformation. *American Journal of Science*, 286, 737-764.
- Kay, S., Coira, B., 2009. Shallowing and steepening subduction zones, continental lithospheric loss, magmatism, and crustal flow under the Central Andean Altiplano-Puna Plateau. In: Kay, S., Ramos, V., Dickinson, W. (eds.). *Backbone of the Americas: shallow subduction, plateau uplift, and ridge and terrane collision*, The Geological Society of America, 204-229.
- Kay, S.M., Mpodozis, C., Coira, B., 1999. Neogene magmatism, tectonism and mineral deposits of the Central Andes (22°-23° S Latitude). In: Skinner, B.J. (ed.). *Geology and Ore Deposits of the Central Andes*. Society of Economic Geologists Special Publication, 7, 27-59.
- Limarino, C., Gutiérrez, P., Malizia, D., Barreda, V., Page, S., Osters, H., Linares, E., 1999. Edad de las secuencias paleógenas y neógenas de las cordilleras de la Brea y Zancarrón, Valle del Cura, San Juan. *Revista de la Asociación Geológica Argentina*, 54, 177-181.
- Litvak, V., 2009. El volcanismo Oligoceno superior – Miocene inferior del Grupo Doña Ana en la Alta Cordillera de San Juan. *Revista de la Asociación Geológica Argentina*, 64, 201-213.
- Litvak, V., Poma, S., 2005. Estratigrafía y facies volcánicas y volcánoclasticas de la Formación Valle del Cura: magmatismo paleógeno en la Cordillera Frontal de San Juan. *Revista de la Asociación Geológica Argentina*, 60, 402-416.
- Maksaev, V., Moscoso, R., Mpodozis, C., Nasi, C., 1984. Las unidades volcánicas y plutónicas del Cenozoico superior en la Alta Cordillera del Norte Chico (29°-31° Sur): Geología, Alteración Hidrotermal y Mineralización. *Revista Geológica de Chile*, 21, 11-51.
- Malizia, D., Limarino, C., Sosa-Gomez, J., Kokot, R., Nullo, E., Gutierrez, P., 1997. Descripción de la Hoja Geológica Cordillera del Zancarrón, escala 1: 100.000. Secretaría de Minería de la Nación, Buenos Aires, unpublished, 280pp.

- McNeice, G.W., Jones, A.G., 2001. Multisite, multifrequency tensor decomposition of magnetotelluric data. *Geophysics*, 66, 158-173.
- Mpodozis, C., Ramos, V.A., 1989. The Andes of Chile and Argentina. In: Ericksen, G.E., Cañas Pinochet, M.T., Reinemud, J.A. (eds.). *Geology of the Andes and its relation to hydrocarbon and mineral resources*, Circumpacific Council for Energy and Mineral Resources, Earth Sciences Series, 11, 59-90.
- Muñoz, G., 2013. Exploring for Geothermal Resources with Electromagnetic Methods. *Survey in Geophysics*, 35, 101-122.
- Newman, G., Gasperikova, E., Høevrsten, G., Wanamaker, P., 2008. Three dimensional magnetotelluric characterization of the Coso geothermal field. *Geothermics*, 37, 369-399.
- Nullo, E., Marín, G., 1990. Geología y estructura de las quebradas de la Sal y de la Ortiga, San Juan. *Revista de la Asociación Geológica Argentina*, 45, 323-335.
- Pesce, A., Miranda, E., 2003. Catálogo de manifestaciones termales de la República Argentina. Servicio Geológico Minero Argentino, Buenos Aires, Instituto de Geología y Recursos Minerales, 165pp.
- Ramos, V.A., 2010. The tectonic regime along the Andes: present-day and Mesozoic regimes. *Geological Journal*, 45, 2-25.
- Ramos, V.A., Kay, S.M., Page, R., Munizaga, E., 1989. La Ignimbrita Vacas Heladas y el cese del volcanismo en el Valle del Cura, provincia de San Juan. *Revista de la Asociación Geológica Argentina*, 44, 336-352.
- Reddy, I., Rankin, D., Phillips, R., 1977. Three-dimensional modelling in magnetotelluric and magnetic variation sounding. *Geophysical Journal of the Royal Astronomical Society*, 5, 13-325.
- Risacher, E., Hauser, A., 2008. Catastro de las principales fuentes de aguas termales de Chile Servicio Nacional de Geología y Minería, unpublished, 81pp.
- Rodi, W., Mackie, R., 2001. Nonlinear conjugate gradients algorithm for 2D magnetotelluric inversion. *Geophysics*, 66, 174-187.
- Simpson, F., Bahr, K., 2005. *Practical Magnetotellurics*. Cambridge, University press, 272pp.
- Smith, J.T., 1995. Understanding telluric distortion matrices. *Geophysical Journal International*, 122, 219-226.
- Spichak, V., Manzella, A., 2009. Electromagnetic sounding of geothermal zones. *Journal of Applied Geophysics*, 68, 459-478.
- Swift, C., 1967. A magnetotelluric investigation of a electrical conductivity anomaly in the southwestern United States. PhD Thesis. Cambridge, Massachusetts Institute of Technology, 226pp.
- Syracuse, E.M., Abers, G.A., 2006. Global compilation of variations in slab depth beneath arc volcanoes and implications. *Geochemistry, Geophysics, Geosystems*, 7, Q05017.
- Winocur, D., 2010. Geología y estructura del Valle del Cura y el sector central del Norte Chico, provincia de San Juan y IV Región de Coquimbo, Argentina y Chile. PhD. Thesis. Buenos Aires, Universidad de Buenos Aires, unpublished, 354pp.
- Winocur, D., Ramos, V., 2011. La Formación Valle del Cura: Su edad y ambiente tectónico. 18° Congreso Geológico Argentino, Actas (Cd-Room), Neuquén.
- Winocur, D., Litvak, V., Ramos, V., 2014. Magmatic and tectonic evolution of the Oligocene Valle del Cura basin, main Andes of Argentina and Chile: Evidence for generalized extension. In: Sepúlveda, S., Giambiagi, L., Pinto, L., Moreiras, S., Tunik, M., Hoke, G., Farías, M. (eds.). *Geodynamic Processes in the Andes of Central Chile and Argentina*. Geological Society of London, Special Publications, 109-130.

Manuscript received August 2018;
revision accepted June 2019;
published Online July 2019.